Grid Generation and Adaptation by Monge-Kantorovich Optimization in Two and Three Dimensions

John M. Finn, Gian Luca Delzanno, and Luis Chacón

T-15, Plasma Theory, Los Alamos National Laboratory, Mail stop: K717, Los Alamos, NM 87545

Summary. The derivation of the Monge-Ampère (MA) equation, as it results from a variational principle involving grid displacement, is outlined in two dimensions (2D). This equation, a major element of Monge-Kantorovich (MK) optimization, is discussed both in the context of grid generation and grid adaptation. It is shown that grids which are generated by the MA equation also satisfy equations of an alternate variational principle minimizing grid distortion. Numerical results are shown, indicating robustness to grid tangling. Comparison is made with the deformation method [G. Liao and D. Anderson, *Appl. Analysis* **44**, 285 (1992)], the existing method of equidistribution. A formulation is given for more general physical domains, including those with curved boundary segments. The Monge-Ampère equation is also derived in three dimensions (3D). Several numerical examples, both with more general 2D domains and in 3D, are given.

1 Introduction

In this paper we describe an approach to grid generation and adaptation in 2D and 3D based on *equidistribution*. This means that we take a monitor function or density $\rho(x, y)$ (in 2D) and find a mapping from the logical space $\boldsymbol{\xi} = (\xi, \eta) \in \Xi$ (the unit square in our case) to the physical domain $\mathbf{x} = (x, y) \in X$ satisfying $\rho(x, y)dxdy = d\xi d\eta$, or $\rho J_0 = 1$, where $J_0 = \partial(x, y)/\partial(\xi, \eta)$ is the Jacobian. Thus the rectangular grid cells in the logical space, all having equal area $d\xi d\eta = dA$, map to physical cells with equal measure $\rho(x, y)dxdy = dA$. In 3D this takes the form $\rho(x, y, z)dxdydz = dV$.

Equidistribution is an important general principle, and has potentially many applications. For example, the density ρ can be an estimate of the error in a numerical scheme. It has been shown that equidistribution of the local error leads to minimization of the global error [1]. Another example consists of compressible hydrodynamics when the sound speed c_s varies greatly over the domain, e. g. due to a large change of density. Then the CFL (Courant-Friedrichs-Lewy) condition for an explicit code $\Delta t \lesssim \Delta x/c_s$, where Δt is the time step and Δx is the grid cell size respectively, can in $1D$ be made uniform over the domain by equidistributing $\rho = 1/c_s$.

In one dimension, the equidistribution requirement $\rho(x)dx = d\xi$ determines $x(\xi)$. In higher dimensions, the equidistribution requirement cannot be satisfied

uniquely. In Sec. 2.1 we introduce a variational principle to determine a unique solution. In this principle, the L_2 norm of the grid displacement is minimized. This leads to the Monge-Ampère (MA) equation. This is a key element of Monge-Kantorovich (MK) optimization, applied here to grid generation and adaptation. In Sec. 2.2 we discuss the relationship with another variational principle based on minimization of the grid distortion, defined as the trace of the covariant metric tensor. Minimization of grid displacement and particularly grid distortion suggest strongly that grids generated by such methods should be robust to tangling.

In Sec. 3 we discuss briefly the numerical methods used, namely multigrid preconditioned Newton-Krylov. In Sec. 4 we show numerical results on the grid produced by the MK method, in 2D with the physical domain X equal to the unit square. We compare these results with the grid produced by the deformation method of Ref. [2], the only other area/volume equidistribution method in the literature. The deformation method is based on finding a flow related to the required Jacobian of the map $\boldsymbol{\xi} \to \mathbf{x}$, and integrating an ODE with that flow. The flow is, however, not unique; in fact in Ref. [2] several examples of such a flow are given. We show that the grid obtained using one of these flows is considerably less smooth than the grid obtained by MK optimization, and more prone to tangling.

In Sec. 5 we formulate the problem in 2D with more general physical domains and show numerical examples. In Sec. 6 we outline the formulation in 3D, with a numerical example. In the Appendix we show some detail related to the analysis in Sec. 2, as a template for the analysis in Sec. 6.

2 Monge-Kantorovich Optimization in 2D

In this section we introduce a variational principle based on Monge-Kantorovich optimization as a method of grid generation and adaptation. We also discuss briefly the relationship with another variational principle based on minimizing the grid distortion, and discuss grid tangling. This material reviews Ref. [3].

2.1 Variational Principle with Local Constraint

Equidistribution of a density $\rho(x, y)$ is determined by the condition $\rho(x, y)dxdy = \rho_0(\xi, \eta)d\xi d\eta$, with $\rho_0(\xi, \eta) = 1$. Here, $\mathbf{x} = (x, y)$ are coordinates on the physical domain X, with bouondary ∂X. Also, $\boldsymbol{\xi} = (\xi, \eta)$ are logical variables on the logical domain Ξ, in our case the unit square $[0, 1] \times [0, 1]$. For grid *generation*, we consider $\psi_0 : \Xi \to X$, with $\rho(x, y)$ specified.

For grid *adaptation*, we consider the sequence $\Xi \to X \to X$, and the map $\psi : X \to X$ giving $\mathbf{x}' = \psi(\mathbf{x})$. See Fig. 1. For adaptation, both $\rho(x, y)$ and $\rho'(x', y')$ are specified. One application is for time-stepping with $\rho(x, y)$ an estimate of the local error of a PDE at time t, and $\rho'(x', y')$ the error estimate at time $t + \Delta t$. Both densities are normalized so that

$$\int \rho(x, y)dxdy = \int \rho'(x', y')dx'dy' = 1. \tag{1}$$

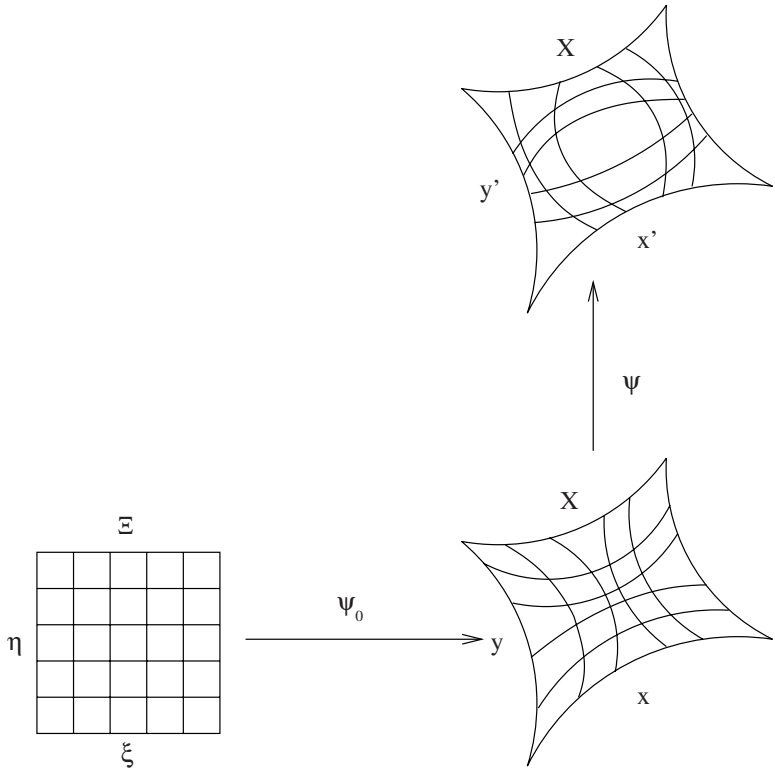

Fig. 1. Sketch of the map ψ_0 from the unit square Ξ to the physical domain X with curved boundary segments, and a second map $\psi : X \to X$

The new density ρ' is also equidistributed if $\rho(x,y)dxdy = \rho'(x',y')dx'dy' = d\xi d\eta$. In terms of the Jacobian J of the map $\psi : \mathbf{x} \to \mathbf{x}' = (x', y')$, this condition takes the form

$$J = \frac{\partial(x',y')}{\partial(x,y)} = \frac{\rho(x,y)}{\rho'(x',y')}. \tag{2}$$

In one dimension, the corresponding equation $\rho(x)dx = \rho'(x')dx'$ has the unique solution (up to an irrelevant integration constant) $R(x) = R'(x')$, where R, R' are cumulative distribution functions. In higher dimensions, Eq. (2) does not have a unique solution. In a time-stepping context, a grid $\mathbf{x}'(\boldsymbol{\xi})$ satisfying Eq. 2 with a large amount of rotation can be very different from $\mathbf{x}(\boldsymbol{\xi})$, even in the extreme case in which ρ and ρ' are equal.

In order to specify a map uniquely and optimally for grid generation and adaptation, we develop a variational principle with Eq. (2) as a constraint. Consider the first variation $\delta \int dxdy\mathcal{L}$ with [3]

$$\begin{aligned}\mathcal{L}(x,y,x',y') = \rho(x,y)\left[(x'-x)^2/2 + (y'-y)^2\right]/2 \\ -\lambda(x,y)\left[\rho'(x',y')\left(\partial_x x'\partial_y y' - \partial_x y'\partial_y x'\right) - \rho(x,y)\right].\end{aligned} \tag{3}$$

This is the standard L_2 form of Monge-Kantorovich optimization [4]. Here, $\lambda(x,y)$ is a local Lagrange multiplier, which ensures that the Jacobian condition (2) holds locally. In the time stepping context, this minimization of the L_2 norm of $\mathbf{x}' - \mathbf{x} = \psi(\mathbf{x}) - \mathbf{x}$ (weighted by ρ) minimizes the *grid velocity*. For the case for which X is the unit square, the boundary conditions on ∂X take a simple form: each side of X maps to itself under ψ. That is, $\hat{\mathbf{n}} \cdot (\mathbf{x}' - \mathbf{x}) = 0$, where $\hat{\mathbf{n}}$ is the vector normal to ∂X. These boundary conditions ensure that the boundary terms obtained by integrating $\delta \int dxdy\mathcal{L}$ by parts vanish [3].

The variation with respect to $\mathbf{x}'$ leads [3] after some analysis to

$$\mathbf{x}' = \mathbf{x} + \nabla\Phi(\mathbf{x}). \tag{4}$$

See the Appendix. That is, ψ is a gradient map $\mathbf{x}' = \nabla\Omega(\mathbf{x})$ with $\Omega(\mathbf{x}) = (x^2+y^2)/2+\Phi(\mathbf{x})$. This is a major conclusion in Monge-Kantorovich optimization theory [4]. Substituting into the Jacobian condition (2), we find

$$\nabla^2_{\mathbf{x}}\Phi + H_{\mathbf{x}}[\Phi] = \frac{\rho(x,y)}{\rho'(x',y')} - 1, \tag{5}$$

where $H_{\mathbf{x}}[\Phi]$ is the Hessian $\partial_{xx}\Phi\,\partial_{yy}\Phi - (\partial_{xy}\Phi)^2$. This is the 2D Monge-Ampère (MA) equation, a single nonlinear equation for $\Phi(x,y)$. (An approximate form of the MA equation was used for grid generation in Ref. [5].) There are two sources of nonlinearity: the Hessian and the dependence of the right side on $\mathbf{x}' = \mathbf{x}+\nabla\Phi$. The above boundary condition $\hat{\mathbf{n}} \cdot (\mathbf{x}' - \mathbf{x}) = 0$ leads to

$$\hat{\mathbf{n}} \cdot \nabla\Phi = 0 \tag{6}$$

on ∂X. It is known that a solution to the MA equation with these boundary conditions exists and is unique, and that the MA equation is elliptic [6].

2.2 Relation with Minimum Distortion

It is plausible that the variational principle using the Lagrangian $\mathcal{L}(x,y,x',y')$ of Eq. (3) should be helpful in preventing grid tangling. In a time-stepping context (for grid adaptation), if the cells are reasonably rectangular at one time, and the L_2 norm of the displacement is minimized, the cells at the next time step are expected to be reasonably rectangular for Δt small, i. e. $\rho(x,y)/\rho'(x',y')$ close to unity.

Based on these thoughts, consider a variational principle minimizing the cell distortion. We define $\mathcal{L}_2(x,y,x',y')$ by

$$\begin{aligned}\mathcal{L}_2(x,y,x',y') &= \rho(x,y)\,(g_{11}+g_{22})\,/2 \\ -\mu(x,y)\,&\left[\rho'(x',y')\,(\partial_x x'\partial_y y' - \partial_x y'\partial_y x') - \rho(x,y)\right],\end{aligned} \tag{7}$$

where $T = g_{11} + g_{22} = (\partial_{x_i} x'_j)(\partial_{x_i} x'_j)$ (summation implied) is the trace of the covariant metric tensor $T = \mathrm{trace}(\mathrm{J}^{\mathrm{T}}\mathrm{J})$. This quantity measures the distortion of the $\mathbf{x}'$ cells relative to the $\mathbf{x}$ cells. Again, $\mu(x,y)$ is a local Lagrange

multiplier, guaranteeing that Eq. (2) holds locally. In Ref. [3] we showed that for $\rho(x, y) = 1 + O(\epsilon)$, $\rho'(x', y') = 1 + O(\epsilon)$ with $\epsilon \ll 1$, solutions of the MA equation are solutions of the variational equations obtained from Eq. (7), i.e. are also minimum distortion solutions. This conclusion is further indication that MA solutions should be robust to tangling. We discuss numerical results related to tangling in Sec. 4.1.

3 Numerical Methods

We solve the MA equation by Jacobian-free Newton-Krylov methods [7, 8]. The particular solver is GMRES [9], preconditioned by multigrid. The fact that the MA equation is elliptic means that multigrid can be used effectively. The function Φ is defined at cell centers and the boundary conditions (6) are implemented using ghost cells in the logical domain Ξ. The efficiency and accuracy of these methods for solving the MA equation have been documented in Ref. [3]. Some of this material is reviewed in the next section.

4 Examples in a Square

Here, we consider X to be the unit square and $\rho(x, y) = 1$. For this case, we will describe the problem as grid adaptation.

4.1 Isotropic Example

The first case we show, from Ref. [3], has density

$$\rho'(x', y') = \frac{C}{2 + \cos(8\pi r')} \tag{8}$$

Table 1. Performance study for the Monge-Kantorovich approach with $\rho'(x', y')$ given by Eq. (8). Shown are the equidistribution error $\sim 1/N_x^2$, for grids with $N_x = N_y$; the CPU time; the grid quality measures $||\mathbf{p}||_2^{MK}$ and $||g_{11} + g_{22}||_1^{MK}$; and the number of linear and nonlinear iterations as functions of $N = N_x \times N_y$.

Number of Cells	**Error**	**CPU time [s]**	$\|\|\mathbf{p}\|\|_2^{MK}$	$\|\|g_{11} + g_{22}\|\|_1^{MK}$	Newton/ GMRES its.
16×16	9.64×10^{-2}	0.1	0.0173	1.449	3/3
32×32	2.28×10^{-2}	0.4	0.0173	1.466	4/4
64×64	5.78×10^{-3}	1.3	0.0173	1.470	4/4
128×128	1.46×10^{-3}	4.9	0.0174	1.470	4/4
256×256	3.67×10^{-4}	19	0.0174	1.471	4/4

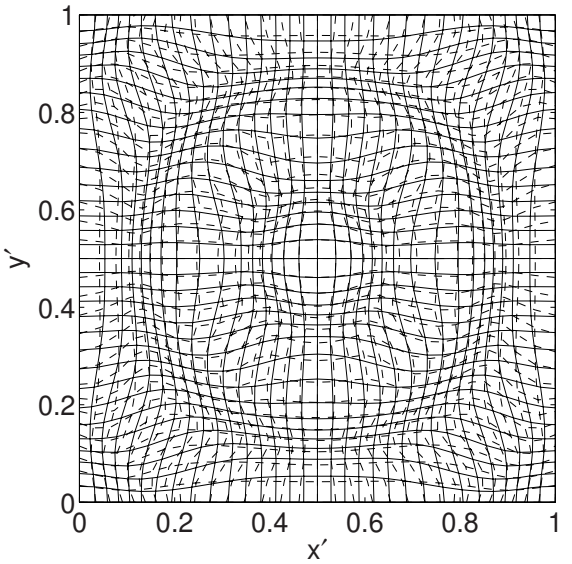

Fig. 2. The grid for Eq. (8) by MK (solid) and by deformation method (dashed)

Table 2. Performance study for the deformation method with time step $\Delta t = 0.01$ for Eq. (8). The grid quality measures $||\mathbf{p}||_2$ and $||g_{11} + g_{22}||_1$ are expressed in terms of variation with respect to the values in Table 1.

Number of Cells	**Error**	**CPU time** [s]	$\frac{\|\|\mathbf{p}\|\|_2}{\|\|\mathbf{p}\|\|_2^{MK}} - 1$	$\frac{\|\|g_{11}+g_{22}\|\|_1}{\|\|g_{11}+g_{22}\|\|_1^{MK}} - 1$
16×16	1.16×10^{-1}	0.2	+24%	+1%
32×32	3.53×10^{-2}	0.9	+28%	+2%
64×64	9.64×10^{-3}	3.4	+30%	+3%
128×128	2.46×10^{-3}	13.6	+30%	+3%
256×256	6.21×10^{-4}	55	+30%	+3%

with $r' = \sqrt{(x' - 1/2)^2 + (y' - 1/2)^2}$. The constant C is determined by normalization as in Eq. (1). The grid is shown in Fig. 2 (solid lines) for 32×32 cells. This isotropic example has $O(1)$ variations in density ($\rho_{max}/\rho_{min} = 3$) over scales $l \sim 0.1$ right up to the boundary. The performance data for this example are shown in Table 1. Note that the computational time required for convergence scales as the total number of grid points $N_x \times N_y$, i. e. it is optimal. This is traced to the fact that the number of Newton and GMRES iterations is nearly independent of the grid refinement.

In Fig. 2 (dashed lines) we have superimposed the grid determined by the deformation method using the proposed symmetric flow of Ref. [2]. It is clear that this grid is not as smooth as the MK grid. Table 2 shows performance for

the deformation method for this example. In particular, note that the L_2 norm of $\mathbf{p} = \mathbf{x}' - \mathbf{x}$ is much larger for the deformation method.

4.2 Anisotropic Example

A second example has

$$\rho'(x', y') = C\left[1 + \frac{9}{1 + 100r'^2\cos^2(\theta' - 20r'^2)}\right]. \tag{9}$$

Here, $r' = \sqrt{(x' - 0.7)^2 + (y' - 0.5)^2}$ and $\theta' = \tan^{-1}[(x' - 0.7)/(y' - 0.5)]$. The 64×64 grid obtained by MK optimization is shown in Fig. 3. This example mimics the spiral pattern that develops in the nonlinear Kelvin-Helmholtz instability. This example has $\rho'_{max}/\rho'_{min} \approx 9$ and very fine scales below $l = 0.02$. This is a very challenging example: the corresponding 64×64 grid obtained by the deformation method tangles [3], but the MK grid is quite smooth.

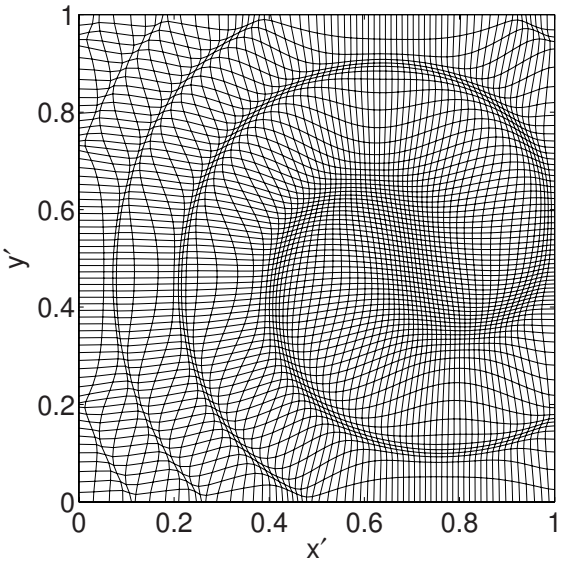

Fig. 3. 64×64 MK grid according to the anisotropic spiral density (9)

4.3 An Example with Fine Structures and Large Jumps in Density

To demonstrate the power of the MK method, we show an example of adapting to challenging images. This is the ubiquitous Lena image [10], commonly used as a standard image for testing image processing methods. We take as density $\rho'(x', y')$ the brightness of the monochrome Lena image. For 200×200 grid points as in Fig. 4, it shows much of the detail in the original image.

Fig. 4. The Lena image by the MK method, with a 200×200 grid

5 Formulation in More General 2D Domains; Examples

We present a formulation for more general physical domains, with examples.

5.1 Map from Logical to Physical Domains; Boundary Formulation

An important issue involves dealing with more general physical domains in 2D. Two questions arise. The first is: How are boundary conditions on an arbitrary shaped domain applied? The second is: Do the terms obtained by integrating by parts as in the variation of $\int dxdy\mathcal{L}$ in Eq. (3) again vanish in this more general setting?

To address the first issue, let us start by considering grid generation, i. e. the map $\psi_0 : \Xi \to X$, for a physical domain X whose boundary ∂X consists of four sides mapped from the four sides of the unit square in the logical space.

See Fig. 1. We shall specialize here to the case in which the four sides of the boundary are given respectively by

$$\begin{array}{rrl} \text{L} - & \text{left side}: & x = x_1(y), \\ \text{R} - & \text{right side}: & x = x_2(y), \\ \text{B} - & \text{bottom}: & y = y_1(x), \\ \text{T} - & \text{top}: & y = y_2(x). \end{array} \tag{10}$$

These boundary conditions on $\Phi(\xi, \eta)$ take the form

$$\begin{aligned} L\ (\xi = 0): &\quad \frac{\partial \Phi}{\partial \xi} = x_1 \left(\eta + \frac{\partial \Phi}{\partial \eta} \right), \\ R\ (\xi = 1): &\quad 1 + \frac{\partial \Phi}{\partial \xi} = x_2 \left(\eta + \frac{\partial \Phi}{\partial \eta} \right), \\ B\ (\eta = 0): &\quad \frac{\partial \Phi}{\partial \eta} = y_1 \left(\xi + \frac{\partial \Phi}{\partial \xi} \right), \\ T\ (\eta = 1): &\quad 1 + \frac{\partial \Phi}{\partial \eta} = y_2 \left(\xi + \frac{\partial \Phi}{\partial \xi} \right). \end{aligned} \tag{11}$$

As in Sec. 2, these boundary conditions require that each side of the square map to the corresponding side of the physical domain, but allow an arbitrary (but one-to-one) motion of points along each of the sides. These nonlinear conditions are applied by solving for the value of Φ in each ghost cell.

For grid adaptation, we deal with the map $\mathbf{x} \to \psi(\mathbf{x}) = \mathbf{x}'$ from X to X, and the corresponding boundary conditions, e. g. $x' = x_1(y')$, in terms of $\Phi(x, y)$, are: are

$$\begin{aligned} L\ (x = x_1(y)): &\quad x_1(y) + \partial_x \Phi(x_1(y), y) = x_1 \left(y + \partial_y \Phi(x_1(y), y) \right), \\ R\ (x = x_2(y)): &\quad x_2(y) + \partial_x \Phi \left(x_2(y), y \right) = x_2 \left(y + \partial_y \Phi(x_2(y), y) \right), \\ B\ (y = y_1(x)): &\quad y_1(x) + \partial_y \Phi(x, y_1(x)) = y_1 \left(x + \partial_x \Phi(x, y_1(x)) \right), \\ T\ (y = y_2(x)): &\quad y_2(x) + \partial_y \Phi(x, y_2(x)) = y_2 \left(x + \partial_x \Phi(x, y_2(x)) \right). \end{aligned} \tag{12}$$

Numerically, these conditions are implemented using ghost cells on the logical domain, by using $[J_0 \equiv \partial(x, y)/\partial(\xi, \eta)]$

$$\begin{aligned} \frac{\partial \Phi}{\partial x} &= \frac{\partial_\xi \Phi\, \partial_\eta y - \partial_\eta \Phi\, \partial_\xi y}{J_0}, \\ \frac{\partial \Phi}{\partial y} &= \frac{-\partial_\xi \Phi\, \partial_\eta x + \partial_\eta \Phi\, \partial_\xi x}{J_0}. \end{aligned} \tag{13}$$

The second issue relates to the terms obtained by integration by parts when taking the Euler-Lagrange equations from the variational principle in Eq. (3). Indeed, we find that the variation of $\int dxdy\mathcal{L}$ contains a term

$$\begin{aligned} -\int dxdy\lambda(x, y)\rho'(x', y')\, &(\partial_x \delta x'\ \partial_y y' - \partial_y \delta x'\ \partial_x y' \\ &+ \partial_x x'\ \partial_y \delta y' - \partial_y x'\ \partial_x \delta y') \end{aligned} \tag{14}$$

in addition to terms proportional to $\delta x'$ and $\delta y'$. Integrating by parts, this expression becomes

$$\int dxdy\,[\delta x'\,(\partial_x(\rho'\lambda\partial_y y') - \partial_y(\rho'\lambda\partial_x y')) + \delta y'\,(\partial_y(\rho'\lambda\partial_x x') - \partial_x(\rho'\lambda\partial_y x'))]$$
$$+ \int dy\lambda(x,y)\rho'(x',y')\,[\partial_y x'\ \delta y' - \partial_y y'\ \delta x']\,|_{x=x_1(y)}^{x=x_2(y)}$$
$$+ \int dx\lambda(x,y)\rho'(x',y')\,[\partial_x y'\ \delta x' - \partial_x x'\ \delta y']\,|_{y=y_1(x)}^{y=y_2(x)}.$$

The analysis involving the first terms (and the other terms proportional to $\delta x'$ and $\delta y'$) proceeds as in Ref. [3] and the Appendix. The terms in the bracket for $x = x_1(y)$, with $x' = x_1(y')$, are

$$\frac{dx_1(y')}{dy'}\frac{\partial y'}{\partial y}\ \delta y' - \frac{\partial y'}{\partial y}\ \frac{dx_1(y')}{dy'}\delta y',$$

which equals zero because $x' = x_1(y')$ implies $\delta x' = (dx_1(y')/dy')\delta y'$. The same is true for the boundary terms at $x = x_2(y)$, $y = y_1(x)$, and $y = y_2(x)$. Therefore the boundary terms obtained by the integration by parts vanish and the analysis proceeds as in Sec. 2.1, the Appendix, and Ref. [3]. In particular, we again conclude that ψ is a gradient map, and that the Monge-Ampère (MA) equation (5) applies.

5.2 Examples with Non-square Physical Domains

The first example, involving grid generation, has a physical domain X consisting of a parallelogram obtained by mapping the sides of the square according to

$$x = a\xi + b\eta, \quad y = b\xi + c\eta, \tag{15}$$

with $a = 1$, $b = 0.2$, and $c = (1 + b^2)/a$. The latter condition ensures that the area of the parallelogram equals unity. The symmetry of this linear map implies that it is a gradient map $\mathbf{x} = \nabla_\xi \Omega$ with $\Omega(\xi,\eta) = a\xi^2/2 + b\xi\eta + c\eta^2/2$. This map is therefore of the form $\mathbf{x} = \boldsymbol{\xi} + \nabla_\xi \Phi(\xi,\eta)$ with

$$\Phi = (a-1)\xi^2/2 + b\xi\eta + (c-1)\eta^2/2. \tag{16}$$

Clearly, $\Phi(\xi,\eta)$ is a solution of the MA equation $\nabla_\xi^2\Phi + H_\xi[\Phi] = \rho_0(\xi,\eta)/\rho(x,y) - 1$ with $\rho_0(\xi,\eta) = \rho(x,y) = 1$. [The determinant condition $c = (1 + b^2/a)$ is not essential: for determinant equal to J_0 (such that $c = (J_0 + b^2)/a$), the MA equation is satisfied with $\rho_0(\xi,\eta) = 1$ and $\rho(x,y) = 1/J_0$.]

From Eq. (15) we conclude that the boundary conditions on the four sides, according to the format of Eq. (10), are

$$\begin{aligned} \mathrm{L}(\xi = 0): &\quad x = x_1(y) = by/c, \\ \mathrm{R}(\xi = 1): &\quad x = x_2(y) = a + b(y-b)/c, \\ \mathrm{B}(\eta = 0): &\quad y = y_1(x) = bx/a, \\ \mathrm{T}(\eta = 1): &\quad y = y_2(x) = c + b(x-b)/a. \end{aligned} \tag{17}$$

We now formulate the problem for grid adaptation, using the MA equation to find the map $\psi : \mathbf{x} \to \mathbf{x}'$ with $\rho(x, y) = 1$ and $\rho'(x', y')$ specified. The boundary conditions are of the form (17) but with $x \to x'$, $y \to y'$. For example, the boundary condition on the left is $x' = by'/c$ or $x + \partial_x \Phi(x, y) = b[y + \partial_y \Phi(x, y)]/c$. From Eq. (17) we conclude $\partial_x \Phi(by/c, y) = b\partial_y \Phi(by/c, y)/c$. Summarizing for the four sides, we obtain

$$\begin{aligned} \text{L}: &\quad \partial_x \Phi(by/c, y) = b\partial_y \Phi(by/c, y)/c, \\ \text{R}: &\quad \partial_x \Phi(a + b(y-b)/c, y) = b\partial_y \Phi(a + b(y-b)/c, y)/c, \\ \text{B}: &\quad \partial_y \Phi(x, bx/a) = b\partial_x \Phi(x, bx/a)/a, \\ \text{T}: &\quad \partial_y \Phi(x, c + b(x-b)/a) = b\partial_x \Phi(x, c + b(x-b)/a)/a. \end{aligned} \tag{18}$$

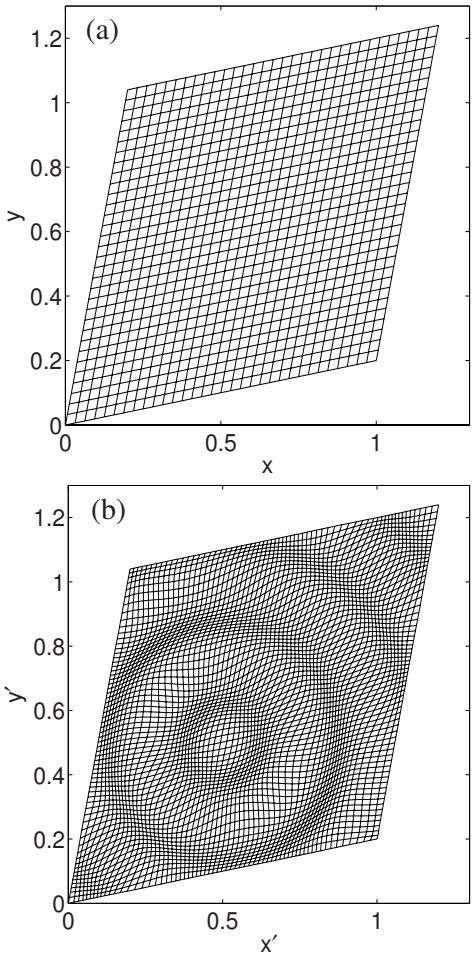

Fig. 5. (a) The linear map $\mathbf{x}(\boldsymbol{\xi})$ [Eq. (15)] from the unit square Ξ to a parallelogram X, with $\rho = 1$; (b) the composite map $\mathbf{x}'(\boldsymbol{\xi}) = \mathbf{x}'(\mathbf{x}(\boldsymbol{\xi}))$ with $\rho'(x', y')$ given by Eq. (8)

Again, these boundary conditions are implemented by means of ghost cells on the logical grid, using Eq. (13).

Results obtained with these boundary conditions for the isotropic case of Eq. (8) are shown in Fig. 5(a) for the (x, y) grid given by Eqs. (15), (16) and in Fig. 5(b) for the (x', y') grid solved numerically. Because the density ρ' is specified as a function of $\mathbf{x}'$, the density of grid lines in Fig. 5(b) is according to Eq. (8), without distortion. In this case, the (x, y) grid (i. e. ψ_0), is formed by a gradient map with $\rho = 1$. (For grid adaptation, it is not necessary that the initial map ψ_0 be a gradient map, i. e. be obtained by MK grid generation.)

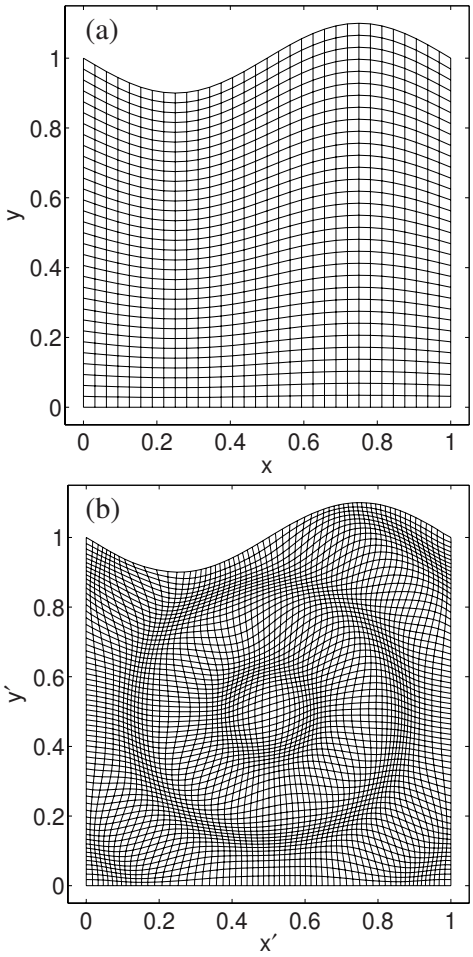

Fig. 6. (a) Sinusoidal map (19) with $\rho = 1$; (b) map obtained by MK grid adaptation with $\rho'(x', y')$ as in Eq. (8)

As a second example, consider X to be the set bounded by $x = 0$; $x = 1$; $y = 0$; $y = 1 - \epsilon \sin(2\pi x)$ for $\epsilon = 0.1$. We choose the 'sinusoidal' map ψ_0 from Ξ to X given by

$$\begin{aligned} x &= \xi, \\ y &= \eta[1 - \epsilon \sin(2\pi\xi)] \end{aligned} \tag{19}$$

and shown in Fig. 6(a). The Jacobian is $J_0 = \partial(x, y)/\partial(\xi, \eta) = 1 - \epsilon \sin(2\pi\xi) = 1 - \epsilon \sin(2\pi x)$. Since $\rho_0(\xi, \eta) = 1$, this implies $\rho(x, y) = [1 - \epsilon \sin(2\pi x)]^{-1}$. The map given by Eq. (19) is not a solution of the MA equation (and is in fact not even a gradient map). However, as we discussed above, this is not an essential requirement for the map ψ_0. For the map $\psi : X \to X$ we specify again $\rho'(x', y')$ according to Eq. (8), and solve the MA equation, Eq. (5). The boundary conditions are of the form (10), (12) with

$$\begin{aligned} \mathrm{L}: &\quad x_1(y) = 0, \\ \mathrm{R}: &\quad x_2(y) = 1, \\ \mathrm{B}: &\quad y_1(x) = 0, \\ \mathrm{T}: &\quad y_2(x) = 1 - \epsilon \sin(2\pi x). \end{aligned} \tag{20}$$

The results, showing the undistorted density of Eq. (8), are in Fig. 6(b).

6 Three Dimensions

In 3D we show that a similar minimization of the L_2 norm of $\mathbf{x}' - \mathbf{x}$ leads to a gradient map and to the 3D generalization of the MA equation. We also show a numerical example obtained by solving the 3D MA equation by methods discussed in Sec. 3.

6.1 Variational Principle and Gradient Map in 3D

In 3D, we will derive the variational principle corresponding to Eq. (3) for general $\rho(x, y, z)$ but for the special case $\rho' = 1$. We have derived the more general case [3], which is tedious and not particularly enlightening. Following the 2D derivation in the Appendix, we have

$$\mathcal{L} = \frac{\rho}{2} (x_i' - x_i)(x_i' - x_i)$$

$$-\lambda(x, y, z) \left[\epsilon_{ijk} \frac{\partial x_i'}{\partial x} \frac{\partial x_j'}{\partial y} \frac{\partial x_k'}{\partial z} - \rho(x, y, z) \right],$$

where ϵ_{ijk} are the components of the usual antisymmetric 3D Levi-Civita tensor, and repeated indices indicate summation. The Euler-Lagrange equations are

$$\rho (x_i' - x_i) + \epsilon_{ijk} \frac{\partial}{\partial x} \left[\lambda \frac{\partial x_j'}{\partial y} \frac{\partial x_k'}{\partial z} \right]$$

$$+\epsilon_{kij}\frac{\partial}{\partial y}\left[\lambda\frac{\partial x'_k}{\partial x}\frac{\partial x'_j}{\partial z}\right]+\epsilon_{jki}\frac{\partial}{\partial z}\left[\lambda\frac{\partial x'_j}{\partial x}\frac{\partial x'_k}{\partial y}\right]=0;$$

the boundary terms and the terms proportional to λ vanish as in the 2D case discussed in the Appendix. We find

$$\rho\,(x'_i-x_i)=-\frac{1}{2}\epsilon_{ijk}\left[\lambda,x'_j,x'_k\right]_{\mathbf{x}},$$

where

$$[f,g,h]_{\mathbf{x}}=\epsilon_{pqr}\frac{\partial f}{\partial x_p}\frac{\partial g}{\partial x_q}\frac{\partial h}{\partial x_r}=\nabla f\cdot\nabla g\times\nabla h.$$

In the next step we show that

$$[f,g,h]_{\mathbf{x}}=J\,[f,g,h]_{\mathbf{x}'}\,. \tag{21}$$

We have

$$[f,g,h]_{\mathbf{x}}=\epsilon_{pqr}\frac{\partial x'_s}{\partial x_p}\frac{\partial x'_t}{\partial x_q}\frac{\partial x'_u}{\partial x_r}\;\frac{\partial f}{\partial x'_s}\frac{\partial g}{\partial x'_t}\frac{\partial h}{\partial x'_u}.$$

Now, since

$$\epsilon_{pqr}\frac{\partial x'_s}{\partial x_p}\frac{\partial x'_t}{\partial x_q}\frac{\partial x'_u}{\partial x_r}=\epsilon_{stu}J,$$

we obtain Eq. (21). Finally, using $\rho=J$ (for $\rho'=1$), this leads to

$$(x'_i-x_i)=-\frac{1}{2}\epsilon_{ijk}\left[\lambda,x'_j,x'_k\right]_{\mathbf{x}'}=-\frac{\partial\lambda}{\partial x'_i}.$$

By following the reasoning at the end of the Appendix, we conclude that Monge-Kantorovich optimization in 3D also leads to a gradient map. This result also holds for general $\rho'(x',y',z')$.

6.2 3D Monge-Ampère Equation

Substituting $\mathbf{x}'=\mathbf{x}+\nabla\Phi(\mathbf{x})$ into the Jacobian equation

$$\frac{\partial(x',y',z')}{\partial(x,y,z)}=\frac{\rho(x,y,z)}{\rho'(x',y',z')},$$

we find

$$\det\begin{bmatrix}1+\partial_{xx}\Phi & \partial_{xy}\Phi & \partial_{xz}\Phi\\ \partial_{yx}\Phi & 1+\partial_{yy}\Phi & \partial_{yz}\Phi\\ \partial_{zx}\Phi & \partial_{zy}\Phi & 1+\partial_{zz}\Phi\end{bmatrix}=\frac{\rho(x,y,z)}{\rho'(x+\partial_x\Phi,y+\partial_y\Phi,z+\partial_z\Phi)}.$$

This is the 3D Monge-Ampère equation (generalizing to arbitrary $\rho'(x',y',z')\neq 1$). When the determinant is expanded out, it has $\nabla^2\Phi$ plus quadratic and cubic terms. The nonlinearities consist of the last two types of terms plus the denominator on the right.

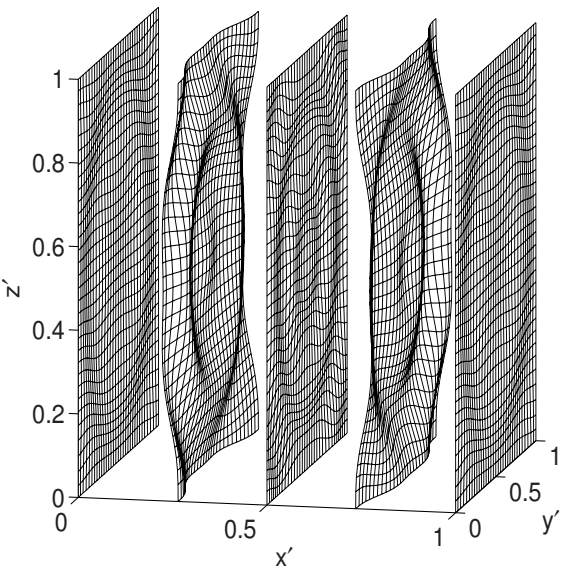

Fig. 7. Grid obtained by the 3D MA equation for the density $\rho'(x', y', z')$ prescribed according to Eq. (22): slices for $x' \approx 0$, 0.25, 0.5, 0.75, 1.0

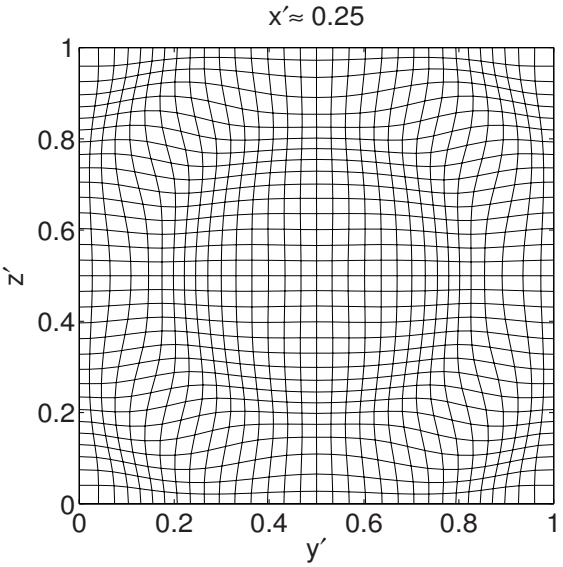

Fig. 8. Grid obtained by 3D MA equation for the density $\rho'(x', y', z')$ prescribed according to Eq. (22): a projection of the grid for $x' \approx 0.25$

6.3 Example in 3D

We treat a case with X the unit cube having $\rho(x, y, z) = 1$ and

$$\rho'(x', y', z') = \frac{C}{2 + \cos(8\pi r')}, \tag{22}$$

now with $r' = \sqrt{(x' - 1/2)^2 + (y' - 1/2)^2 + (z' - 1/2)^2}$. We show the mesh in (x', y', z') in Fig. 7, and Fig. 8 shows a projection of the mesh for $x' \approx 0.25$.

7 Conclusions

We have given a brief review of the main results of Ref. [3] in a square in 2D, showing how minimization of the L_2 norm of the grid displacement leads to equidistribution via the Monge-Ampère (MA) equation, a major element in Monge-Kantorovich (MK) optimization. (Detailed algorithmic issues were discussed in Ref. [3]). We have also shown the relation with minimum distortion and grid tangling. We have exhibited several examples showing how this method works, and comparing it with the deformation method of Ref. [2]. Table 1 and the performance tests in Ref. [3] show that the MK method uses a small amount of computer time and scales optimally with respect to grid size. The results of Ref. [3] also show that the method is robust in two important senses: (1) the increase in computational requirements with the complexity of the error measure $\rho'(x', y')$ is modest and (2) in very challenging densities $\rho'(x', y')$ the grid was not observed to fold.

We have shown new results in 2D on the formulation and application of the MK method in a more general class of physical domains X. The examples of applications include a parallelogram and an area with a sinusoidal boundary segment. These results suggest strongly that the method extends readily to more general physically realistic domains in 2D for grid generation and adaptation. Further work is underway to assess the difficulties involved with multiple block structured grids and unstructured grids.

We have shown a derivation of the Monge-Ampère equation in 3D. We have obtained results using this 3D Monge-Ampère equation in the unit cube.

Acknowledgements. We wish to thank P. Knupp, D. Knoll, G. Hansen, and X. Z. Tang for useful discussions.

References

1. Lapenta, G.: Variational grid adaptation based on the minimization of local truncation error: Time independent problems. J. Comput. Phys. 193, 159 (2004)
2. Liao, G., Anderson, D.: A new approach to grid generation. Appl. Anal. 44, 285–297 (1992)
3. Delzanno, G.L., Chacón, L., Finn, J.M., Chung, Y., Lapenta, G.: An optimal robust equidistribution method for two-dimensional grid generation based on Monge-Kantorovich optimization. J. Comp. Phys. (submitted, 2008)
4. Evans, L.C.: Partial differential equations and Monge-Kantorovich mass transfer. In: Yau, S.T. (ed.) Current Developments in Mathematics (1997)

5. Budd, C.J., Williams, J.F.: Parabolic Monge-Ampère methods for blow-up problems in several spatial dimensions. J. Phys. A 39, 5425 (2006)
6. Caffarelli, L., Nirenberg, L., Spruck, J.: The Dirichlet problem for nonlinear 2nd-order elliptic equations I. Monge-Ampère equation. Communications on Pure and Applied Mathematics 37(3), 369–402 (1984)
7. Kelley, C.T.: Iterative Methods for Linear and Nonlinear Equations. SIAM, Philadelphia (1995)
8. Dembo, R., Eisenstat, S., Steihaug, R.: Inexact Newton methods. J. Numer. Anal. 19, 400 (1982)
9. Saad, Y., Schultz, M.H.: GMRES: a generalized minimal residual algorithm for solving nonsymmetric linear systems. SIAM journal on scientific and statistical computing 7(3), 856–869 (1986)
10. `http://ndevilla.free.fr/lena/`

Appendix

In this appendix we show some technical details relating to minimization of $\int dxdy\mathcal{L}$ in 2D. This is a more compact version of the derivation in Ref. [3], and for our purposes here is a template for the 3D derivations in Sec. 6.

In 2D for the special case $\rho' = 1$, take (with summation notation)

$$\mathcal{L}(\mathbf{x}, \mathbf{x}') = \frac{1}{2}\rho(x,y)(x'_i - x_i)(x'_i - x_i) \qquad (23)$$
$$-\lambda(\mathbf{x})\left[\epsilon_{ij}\frac{\partial x'_i}{\partial x}\frac{\partial x'_j}{\partial y} - \rho(\mathbf{x})\right],$$

where $\epsilon_{11} = \epsilon_{22} = 0$; $\epsilon_{12} = -\epsilon_{21} = 1$. [The Jacobian $J(\mathbf{x}) = \partial(x', y')/\partial(x, y)$ can be written in any of the alternate forms: $J = [x', y']_{\mathbf{x}}$, where $[\cdot, \cdot]$ is the Poisson bracket; $J = \epsilon_{ij}(\partial x'_i/\partial x)(\partial x'_j/\partial y)$; or $J = \epsilon_{ij}(\partial x'/\partial x_i)(\partial x'/\partial x_j)$.] The Euler-Lagrange equations give

$$\frac{\partial \mathcal{L}}{\partial x'_i} - \frac{\partial}{\partial x_k}\frac{\partial \mathcal{L}}{\partial(\partial x'_i/\partial x_k)} = \qquad (24)$$
$$\rho(\mathbf{x})(x'_i - x_i) + \epsilon_{ij}\frac{\partial \lambda}{\partial x}\frac{\partial x'_j}{\partial y} - \epsilon_{ij}\frac{\partial \lambda}{\partial y}\frac{\partial x'_j}{\partial x} = 0.$$

The terms proportional to λ cancel. The boundary terms take the form

$$-\int dy\left[\lambda\epsilon_{ij}\frac{\partial x'_j}{\partial y}\delta x'_i\right]_{x=0}^{x=1} - \int dx\left[\lambda\epsilon_{ij}\frac{\partial x'_i}{\partial x}\delta x'_j\right]_{y=0}^{y=1}, \qquad (25)$$

each term of which equals zero. Note the Poisson bracket relation $[f, g]_{\mathbf{x}} = J[f, g]_{\mathbf{x}'}$, which follows from

$$[f,g]_{\mathbf{x}} = \epsilon_{kl}\frac{\partial f}{\partial x_k}\frac{\partial g}{\partial x_l} = \epsilon_{kl}\frac{\partial x'_m}{\partial x_k}\frac{\partial f}{\partial x'_m}\frac{\partial x'_n}{\partial x_l}\frac{\partial g}{\partial x'_n} = [x'_m, x'_n]_{\mathbf{x}}\frac{\partial f}{\partial x'_m}\frac{\partial g}{\partial x'_n}$$
$$= \epsilon_{mn}J\frac{\partial f}{\partial x'_m}\frac{\partial g}{\partial x'_n} = J[f,g]_{\mathbf{x}'}.$$

This and the relation $\rho = J$ (for $\rho' = 1$) show that Eq. (24) becomes

$$x_i' - x_i = -\epsilon_{ij}[\lambda, x_j']_{\mathbf{x}'}.$$

The whole point of writing the Poisson bracket in terms of $\mathbf{x}'$ is that this can be rewritten as

$$\begin{aligned} x_i' - x_i &= -\epsilon_{ij}\epsilon_{kl}(\partial\lambda/\partial x_k')(\partial x_j'/\partial x_l') \\ &= -\epsilon_{ij}\epsilon_{kj}(\partial\lambda/\partial x_k') \\ &= -\partial\lambda/\partial x_i'. \end{aligned} \tag{26}$$

This equation shows that $x_i = \partial\left(x_j' x_j'/2 - \lambda\right)/\partial x_i'$. That is, the map ψ^{-1} is a gradient map (a Legendre transform). This implies that ψ is also a gradient map and can be written in the form used in Sec. 2,

$$\mathbf{x}' = \nabla\Omega(\mathbf{x}) = \mathbf{x} + \nabla\Phi(\mathbf{x}).$$